Research paper

Multiscale modeling and simulation of soft adhesion and contact of stem cells

Xiaowei Zeng, Shaofan Li*

Department of Civil and Environmental Engineering, University of California, Berkeley, CA 94720, USA

ABSTRACT

Recently, we have developed a multiscale soft matter model for stem cells or primitive cells in general, aiming at improving the understanding of mechanotransduction mechanism of cells that is responsible for information exchange between cells and their extracellular environment. In this paper, we report the preliminary results of our research on multiscale modeling and simulation of soft contact and adhesion of cells. The proposed multiscale soft matter cell model may be used to model soft contact and adhesion between cells and their extracellular substrates. This model is a generalization of the Fluid Mosaic Model (Singer and Nicolson, 1972), or an extension of Helfrich's liquid crystal membrane model (Helfrich, 1973). To the best of the authors' knowledge, this may be the first time that a soft matter model is developed for cell contact and adhesion. Moreover we have developed and implemented a Lagrange type meshfree Galerkin formulation and the computational algorithm for the proposed cell model. Comparison study with experimental data has been conducted to validate the parameters of the model. By using the soft matter cell model, we have simulated the soft adhesive contact process between cells and their extracellular substrates. The simulation shows that the cell can sense substrate elasticity by responding in different manners from cell spreading motion to cell contact configurations.

© 2010 Elsevier Ltd. All rights reserved.

1. Introduction

Stem cells are unspecific cells that have two defining properties: (1) they have the ability to differentiate into all other functional cells in human body, and (2) they have the ability to self-regenerate. Even though it is generally believed that transcription regulation, or genetic factor, plays an important role in this decision-making process, neither the topology nor the dynamics of the regulatory networks are known at the moment.

Recent developments on stem cell research have revealed that the fate or lineage specification of stem cells depends sensitively on both the rigidity as well as surface microstructure of the extracellular matrix (ECM). For example Discher et al. (2005) and Engler et al. (2006) reported that matrix elasticity directs stem cell lineage specification. Rehfelt et al. (2007) reported that results with drug treatments of various cells on soft, stiff, and rigid matrices show a broad range of possible matrix-dependent drug responses; and cells on soft gels might be relatively unaffected in cell spreading or apoptosis induction whereas cells on stiff substrates seem more sensitive to diverse drugs in terms of spreading. All these indicate a significant influence of matrix elasticity on

---

* *Corresponding author.*
  E-mail address: shaofan@berkeley.edu (S. Li).

cell contact or adhesion, and subsequent cytoskeleton re-organization.

To study the influences of bio-mechanical niche factors on the fate of stem cells will eventually help the development of synthetic niches that may cultivate or trigger stem cells to differentiate into the desirable functional cells (Discher et al., 2009). Because of its scientific and clinic importance, a major focus of molecular cell biology is the study of mechanotransduction effect of cells, in particular stem cells (see Wang et al., 2009, Chien, 2007 and Bao and Suresh, 2003). As pointed out in Wozniak and Chen (2009): *Two main factors contribute to the mechanical stresses that are experienced by cells and influence cell behavior in early development are the mechanical stiffness of the local tissue environment and the contractile activity of the cells that are pulling on that environment. Stiffness and contractility both contribute to the cellular mechanical stresses that are essential for mechanotransduction. Cells routinely contract to pull on the scaffolds to which they are attached (the extracellular matrix (ECM) or other cells), thereby generating tension in the cell (internal mechanical stress). The magnitude of such stress is affected both by the strength of contractile activity in the cell and the substrate stiffness.*

Thus understanding the interplay between cellular contractile activity, stiffness of surrounding tissues and the resulting mechanical deformations and stresses is crucial for establishing a mechanotransduction model. The physical process of mechanotransduction is through contact and adhesion between cells and their extracellular environment. Recently, several models of cell contact and formation of focal adhesion have been proposed, notably Freund and Lin (2004), Ni and Chiang (2007), and Deshpande et al. (2008). Continuum models also have been developed recently to predict cell adhesion in the early stage (see Liu et al., 2007, Cheng et al., 2009 and Sun et al., 2009).

In order to understand the precise mechanical factors in cell contact, adhesion, and sensing process, and to explain the possible mechanotransduction mechanism, recently we have developed a soft matter cell model for study of cell contact and adhesion. This paper reports the preliminary results of this study.

The paper is organized in six sections: in Section 2 we shall report the construction of our soft mater cell and extracellular matrix model; Section 3 is focused on the meshfree implementation of the computational cell model, in Section 4 we shall discuss the Cell adhesion and contact algorithms; and in Section 5, validation of the cell model and a few numerical simulations are provided, and finally in Section 6 we shall discuss some important issues of the soft matter cell model.

2. Cell and ECM modeling

The main objective of this work is to advance stem cell modeling and cell modeling in general, we systematically build a soft matter cell model by treating stem cells as soft matters. A multi-component cell model with a coarse-grained adhesive body force is proposed.

2.1. Basic hypothesis and assumptions

The cell membrane is basically a lipid bilayer. Up to today, the most successful cell model is the fluid mosaic model — the lipid bilayer model (Singer and Nicolson, 1972). It captures two essential features of the lipid bilayer: fluidity and diffusion.

A well-established and very successful mechanics or mathematics model for the cell membrane is Helfrich's liquid crystal cell membrane model (Helfrich, 1973), which is based on or built on the fluid mosaic model. Because Helfrich's liquid crystal cell membrane model has successfully predicted the bi-concave shape of red blood cells, it has been regarded as the first triumph of soft matter physics. This is because the microstructure of the liquid crystal, especially that of Smectic-A liquid crystals, resembles that of the lipid bilayer of cells. In fact, many view the lipid bilayer as a form of bio-liquid-crystal. However, three decades after the Singer–Nicolson model, new evidences have shown that the freedom of proteins on cell membrane are far from unrestricted e.g. Vereb et al. (2003). Damjanovich et al. (1997) showed that the emerging evidence on hierarchically built super-structured protein complexes, which may hinder the diffusion of proteins in the membrane. Dietrich et al. (2002) and Jacobson et al. (1995) have pointed out: "*Most membrane proteins do not enjoy the continuous unrestricted lateral diffusion . . . . Instead, proteins diffuse in a more complicated way that indicates considerable lateral heterogeneity in membrane structure, at least on a nanometer scale*".

From structure viewpoint, a cell consists of membrane wall, cytoplasm, microtubes, cell nucleus, and cytoskeleton — cell's scaffold. The cell nucleus plays a central role in the response to mechanical forces (Caille et al., 2002). According to Maniotis et al. (1997), the nucleus inside the cell is about 9 times stiffer than the cytoplasm. Based on these observations, we propose to model the cell nucleus as hyperelastic materials, which has been used in Caille et al. (2002) to model the nucleus of endothelial cells. To extend Helfrich's liquid crystal membrane model, we propose to use a bulk nematic liquid crystal material to model the outer layer of the cells.

The rational for such soft matter cell model is that cell cytoplasm does not just consist of liquid, it contains cell organelles and many weakly cross-linked polymer networks, such as actin filaments or intermediate filaments. Depending on the types of cells, the content, i.e. microstructure, as well as the concentration of these filaments may be different. In this work, since we are only interested in modeling stem cells, for stem cells, the cell cytoskeleton may be less developed than that of other functional cells. Therefore, the cytoplasm region of the stem cell contains less cytoskeleton but more liquid. Hence, the liquid crystal model may be also suitable for modeling cell cytoplasm region. For simplicity, in this two-layer cell model, we do not distinguish the cell membrane and cell cytoplasm in the present paper as a preliminary study. A refined soft matter model that distinguishes the cell membrane and cell cytoplasm will be reported in a separated paper.

The extracellular matrix is modeled as a substrate of hyperelastic block, which has been extensively used as cell models or gel models (see Sen et al., 2009 and Fereol et al.,
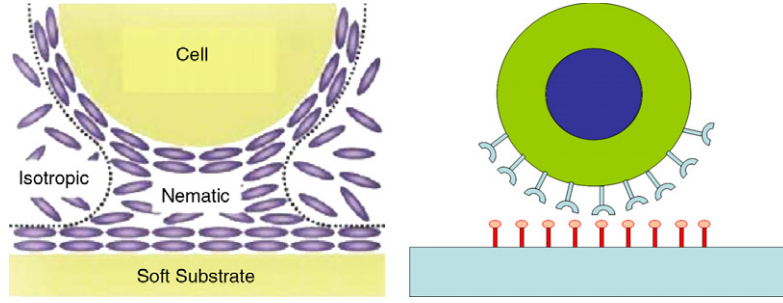
Fig. 1 – Soft matter cell model and soft adhesive contact model.

2009). An illustration of the cell model is shown in Fig. 1. In the following sections, we shall described both the hyperelastic constitutive model and the liquid crystal model used in our cell and extracellular matrix modeling.

2.2. Hyperelastic model

Inside a cell, we use hyperelastic constitutive model to represent cell scaffold and cell plasma aggregates, which are isotropic and nonlinear, and exhibit elastic response of large strains. For hyperelastic material, we adopted the modified Mooney–Rivlin material (Fried and Johnson, 1988) to model the cell nucleus and extracellular matrix. The strain energy density function W for the modified Mooney–Rivlin material is given as

$$W = C_1(I_1 - 3I_3^{1/3}) + C_2(I_2 - 3I_3^{2/3}) + \frac{1}{2}\lambda(\ln I_3)^2 \tag{1}$$

where C_1, C_2 and λ are material constants and $\mathbf{C} = \mathbf{F}^T \cdot \mathbf{F}$ is the right Cauchy–Green deformation tensor; and the three invariants of the right Cauchy–Green tensor are defined as

$$I_1 = tr(\mathbf{C}) \tag{2}$$

$$I_2 = \frac{1}{2}[(tr(\mathbf{C}))^2 - tr(\mathbf{C}^2)] \tag{3}$$

$$I_3 = det(\mathbf{C}). \tag{4}$$

The corresponding constitutive relations can be expressed in terms of the second Piola–Kirchhoff stress tensor $\mathbf{S}$, and the invariants of the right Cauchy–Green tensor,

$$\mathbf{S} = 2\{(C_1 + C_2 I_1)\mathbf{I} - C_2\mathbf{C} - (C_1 I_3^{1/3} + 2C_2 I_3^{2/3} - \lambda \ln I_3)\mathbf{C}^{-1}\}. \tag{5}$$

After the second Piola–Kirchhoff stress is obtained, the first Piola–Kirchhoff stress tensor can be immediately computed as $\mathbf{P} = \mathbf{S} \cdot \mathbf{F}^T$, which can then be substituted into the later developed meshfree Galerkin formulation to calculate the internal nodal force.

If the substrate is modeled as a Mooney–Rivlin hyperelastic medium, its elastic stiffness tensor is a fourth-order tensor that can be evaluated as

$$\mathbb{C} = 4\frac{\partial^2 W}{\partial \mathbf{C}\partial \mathbf{C}} = 4C_2\mathbf{I} \otimes \mathbf{I} + \frac{4}{3}(C_1 I_3^{1/3} + 4C_2 I_3^{2/3} - \lambda)\mathbf{C}^{-1} \otimes \mathbf{C}^{-1}$$
$$- 4(C_1 I_3^{1/3} + 2C_2 I_3^{2/3} - \lambda \ln I_3)\mathbf{C}^{-1} \odot \mathbf{C}^{-1} - 4C_2\mathbb{I}. \tag{6}$$

By making the elastic constants, C_1, C_2 and λ, dependent on spatial coordinates, one can model the substrate with inhomogeneous stiffness.

2.3. Liquid crystal model

Liquid crystal is a typical complex fluid, and its microstructure, especially that of Smectic-A liquid crystal, resembles that of the lipid bilayer of cells. In this work, we adopt a simplified version of the Ericksen–Leslie theory (Lin and Liu, 2000) as the governing equations for the nematic liquid crystal that is used in the proposed cell modeling. The strong forms of the simplified Ericksen–Leslie theory are

$$\rho_0 \frac{D\mathbf{v}}{Dt} = \nabla \cdot \boldsymbol{\sigma} + \mathbf{b}, \quad \forall \mathbf{x} \in V(t) \tag{7}$$

$$\rho_0^d \frac{D\tilde{\mathbf{h}}}{Dt} = \gamma\{\nabla \cdot \nabla \otimes \mathbf{h} - \mathbf{r}(\mathbf{h})\}, \quad \forall \mathbf{x} \in V(t) \tag{8}$$

where $\mathbf{v}$ is the velocity field, $\mathbf{h}$ is the Nematic liquid crystal director field, $\mathbf{b}$ is the body force in the current configuration, ρ_0 and ρ_0^d are density of fluid and director fields in the reference configuration, where the differential gradient operator is acting in the spatial configuration, i.e. $\nabla := \frac{\partial}{\partial x_i}\mathbf{e}_i$; γ is the director elastic constant, $\mathbf{r}$ is a Landau–Ginzburg type potential that governs the evolution of the director field

$$\mathbf{r} = \frac{dR(\mathbf{h})}{d\mathbf{h}} = \frac{\mathbf{h}}{\epsilon^2}(|\mathbf{h}|^2 - 1), \quad \text{and} \quad R(\mathbf{h}) = \frac{1}{4\epsilon^2}(|\mathbf{h}|^2 - 1)^2 \tag{9}$$

and the Cauchy stress is determined as

$$\boldsymbol{\sigma} = -p\mathbf{I} + 2\mu\mathbf{d} - \eta\nabla \cdot (\nabla \otimes \mathbf{h} \odot \nabla \otimes \mathbf{h}) - \tilde{\boldsymbol{\sigma}}. \tag{10}$$

In Eq. (10), $p = \kappa(1 - J)$ is the hydrostatic pressure, κ is the bulk modulus, $J = det(\mathbf{F})$, μ is viscosity, η is a positive constant, and $\tilde{\boldsymbol{\sigma}}$ is the contribution from the contact boundary condition, which can be expressed as

$$\tilde{\boldsymbol{\sigma}} = \begin{cases} A(\mathbf{h} \cdot \nabla\varphi_S)\mathbf{h} \otimes \nabla\varphi_S & \text{planar anchoring} \\ A[(\mathbf{h} \cdot \mathbf{h})\nabla\varphi_S - (\mathbf{h} \cdot \nabla\varphi_S)\mathbf{h}] \otimes \nabla\varphi_S \\ \qquad \text{homeotropic anchoring} \end{cases} \tag{11}$$

where A is a contact constant. A Lagrangian level-set field variable, φ_c, is used to characterize the contact interface location and distribution, and it is chosen as the summation of all meshfree interpolant shape functions in the extracellular matrix,

$$\varphi_S(\mathbf{x}, t) = \sum_{I=1}^{N_s} N_I(\mathbf{X}), \quad \forall \mathbf{X} \in V_{ECM}. \tag{12}$$

Since in the interior of cell,

$$\sum_{I=1}^{N_s} N_I(\mathbf{X}) \equiv 0 \Rightarrow \nabla\varphi_S \equiv 0, \quad \forall \mathbf{X} \in \overset{\circ}{V}_{cell}.$$

However, around the contact region of the cell,

$$\sum_{I=1}^{N_s} N_I(\mathbf{X}) \neq 0 \Rightarrow \nabla \varphi_s \neq 0$$

and its contribution provides the contact force contribution from the director field.

Note that we may construct another Lagrangian level-set field,

$$\varphi_c(\mathbf{X}, t) = \sum_{I=1}^{N_c} N_I(\mathbf{X}), \quad \forall \mathbf{X} \in V_{cell}$$

by using the meshfree shape functions in the cell, and we can use it to replace the director elastic constant γ as

$$\gamma(\mathbf{X}) \to \gamma \varphi_c. \tag{13}$$

Since the meshfree interpolants are a partition of unity inside the cell (Li and Liu, 2004),

$$\varphi_c(\mathbf{X}) = \sum_{I=1}^{N_c} N_I(\mathbf{X}) = 1, \quad \forall \mathbf{X} \in \mathring{V}_{cell}$$

it makes $\gamma(\mathbf{X}) = \gamma$ in the interior of the cell, and at the boundary of the cell, elastic contact will change gradually to zero. Note that the advantage to have φ_c available will make the calculation of cell surface curvature easy, and it is needed for the surface tension calculation in the part where the cell is in contact with ambient atmosphere. The atmosphere contact condition is

$$\boldsymbol{\sigma} \cdot \mathbf{n} = -(\sigma_0 \kappa + p_{air})\mathbf{n}, \quad \forall \mathbf{X} \in \Gamma_{cell/air} \tag{14}$$

where σ_0 is the surface tension, p_{air} is atmosphere pressure, and $\Gamma_{cell/air}$ is the interface between the cell and atmosphere. The principal surface curvature of the cell may be approximated as

$$\kappa = \nabla_x \cdot \mathbf{n} \tag{15}$$

where $\mathbf{F} = \frac{\partial \mathbf{x}}{\partial \mathbf{X}}$ is the deformation gradient.

Remarks 1. $\frac{D\tilde{\mathbf{h}}}{Dt}$ is the objective rate, and it can be any of the following rates,

(a). The convected rate : $\overset{\circ}{\mathbf{h}} = \frac{D\mathbf{h}}{Dt} + \boldsymbol{\ell}^T \cdot \mathbf{h}$;

(b). The corotational rate : $\overset{\triangle}{\mathbf{h}} = \frac{D\mathbf{h}}{Dt} - \mathbf{w} \cdot \mathbf{h}$;

where $\boldsymbol{\ell}$ is the velocity gradient, and $\mathbf{w}$ is the spin tensor,

$$\boldsymbol{\ell} = \dot{\mathbf{F}} \mathbf{F}^{-1}$$
$$\mathbf{w} = \frac{1}{2}(\boldsymbol{\ell} - \boldsymbol{\ell}^T).$$

3. Meshfree Galerkin formulation and the computational algorithm

A total Lagrangian formulation is adopted in the numerical computation. The numerical simulations are conducted by using meshfree methods (Li and Liu, 2004). Meshfree method have advantages for treating large deformation problems comparing with traditional finite element method. In our meshfree simulation, both the cell and its substrate are
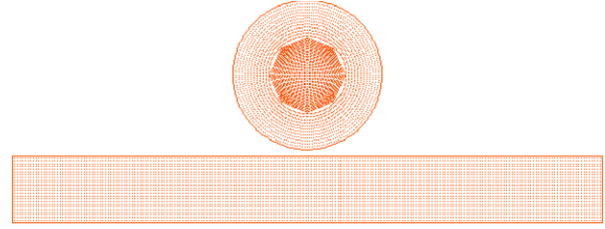
Fig. 2 – Meshfree discretization of the cell and extracellular matrix model.

discretized by a set of particles and then they are represented by interpolation functions (see Fig. 2).

The weak form of the balance of linear momentum under finite strain condition can be expressed as

$$\sum_{i=1}^{2} \int_{\Omega_0^{(i)}} \rho_0^{(i)} \ddot{\mathbf{u}}^{(i)} \cdot \delta \mathbf{u}^{(i)} d\Omega^{(i)} + \sum_{i=1}^{2} \int_{\Omega_0^{(i)}} \mathbf{P}^{(i)} : \delta \mathbf{F}^{(i)} d\Omega^{(i)}$$

$$= \sum_{i=1}^{2} \int_{\Omega_0^{(i)}} \rho_0^{(i)} \mathbf{B}^{(i)} \cdot \delta \mathbf{u}^{(i)} d\Omega^{(i)}$$

$$+ \sum_{i=1}^{2} \int_{\Gamma_t^{(i)}} \bar{\mathbf{T}}^{(i)} \cdot \delta \mathbf{u}^{(i)} dS^{(i)} + \sum_{i=1}^{2} \delta \Pi_{AC}^{(i)} \tag{16}$$

where $\mathbf{B}$ is the body force, $\mathbf{P}$ is the first Piola–Kirchhoff stress, $\bar{\mathbf{T}}$ is the prescribed traction on the traction boundary $\Gamma_t^{(i)}$, $i = 1$ corresponding to cell and $i = 2$ corresponding to extracellular matrix substrate. Note the last terms in Eq. (16), $\delta \Pi_{AC}^{(i)}$, denote the virtual work contribution from adhesive contact, which will be discussed in details in the next Section.

The nematic director evolution is only for cell, for simplicity, we do not introduce $i = 1$ in the formulation, a weak form of the governing equation can be derived as:

$$\int_{\Omega_0} \rho_0^d J \frac{D\mathbf{h}}{Dt} \cdot \delta \mathbf{h} d\Omega$$

$$= -\int_{\Omega_0} \gamma \{(\mathbf{F}^{-1} \cdot \mathbf{F}^{-T}) \cdot (\nabla_X \otimes \mathbf{h})\} : (\nabla_X \otimes \delta \mathbf{h}) d\Omega$$

$$+ \int_{\Gamma_t} \gamma \{\mathbf{N} \cdot (\mathbf{F}^{-1} \cdot \mathbf{F}^{-T}) \cdot (\nabla_X \otimes \mathbf{h})\} \cdot \delta \mathbf{h} dS$$

$$+ \int_{\Gamma_c} \gamma \{\mathbf{N} \cdot (\mathbf{F}^{-1} \cdot \mathbf{F}^{-T}) \cdot (\nabla_X \otimes \mathbf{h})\} \cdot \delta \mathbf{h} dS$$

$$- \int_{\Omega_0} \gamma J \mathbf{r}(\mathbf{h}) \cdot \delta \mathbf{h} d\Omega \tag{17}$$

where Γ_c denotes the contact boundary. By assuming that

$$\mathbf{N} \cdot (\mathbf{F}^{-1} \cdot \mathbf{F}^{-T}) \cdot (\nabla_X \otimes \mathbf{h}) = 0, \quad \forall \mathbf{x} \in \Gamma_t$$

and

$$\mathbf{h} = \bar{\mathbf{h}} \Rightarrow \delta \mathbf{h} = 0, \quad \forall \mathbf{x} \in \Gamma_c.$$

Consider the following meshfree interpolation,

$$\mathbf{u}(\mathbf{X}, t) = \sum_{I=1}^{n_{node}} N_I(\mathbf{X}) \mathbf{d}_I(t) \tag{18}$$

$$\mathbf{h}(\mathbf{X}, t) = \sum_{I=1}^{n_{node}} N_I(\mathbf{X}) \mathbf{h}_I(t). \tag{19}$$

Note that even though, the director field, $\mathbf{h}(X, t)$, is essentially a part of displacement gradient. The robustness of meshfree

computation allows us to use equal-order interpolation without cause severe numerical instability.

Following the standard meshfree discretization procedure, e.g. Li and Liu (2004), we can obtain the following discrete equations of motion with the understanding that those equations of motions applied to both cell and substrate:

$$\mathbf{M}\ddot{\mathbf{d}} = \mathbf{f}^{ext} - \mathbf{f}^{int}(\mathbf{d}) \tag{20}$$

where $\mathbf{M}$ is the lumped mass matrix, $\mathbf{f}^{int}$ is the internal force array arising from the current state of stress, $\mathbf{f}^{ext}$ is the external force array including body forces and surface traction and contact forces,

$$\mathbf{M}_{IJ} = \int_{\Omega_0} \rho_0 \mathbf{N}_I \mathbf{N}_J d\Omega \tag{21}$$

$$\mathbf{f}_I^{int} = \int_{\Omega_0} P_{ij} \mathbf{N}_{I,J} \mathbf{e}_i d\Omega \tag{22}$$

$$\mathbf{f}_I^{ext} = \int_{\Omega_0} \rho_0 \mathbf{B}_i \mathbf{N}_I \mathbf{e}_i d\Omega + \int_{\Gamma_t} \bar{\mathbf{T}}_i \mathbf{N}_I \mathbf{e}_i dS + \int_{\Gamma_c} \bar{\mathbf{f}}_i \mathbf{N}_I \mathbf{e}_i dS. \tag{23}$$

At time $t_{n+1} = t_n + \Delta t$, the discrete equation of motion can be written as:

$$\mathbf{M}\mathbf{a}_{n+1} = \mathbf{f}_{n+1}^{ext} - \mathbf{f}_{n+1}^{int}. \tag{24}$$

If the central difference scheme is used in the time integration, we have

$$\mathbf{d}_{n+1} = \mathbf{d}_n + \Delta t \mathbf{v}_n + \frac{1}{2}\Delta t^2 \mathbf{a}_n \tag{25}$$

$$\mathbf{a}_{n+1} = \mathbf{M}^{-1}(\mathbf{f}_{n+1}^{ext} - \mathbf{f}_{n+1}^{int}) \tag{26}$$

$$\mathbf{v}_{n+1} = \mathbf{v}_n + \frac{1}{2}\Delta t(\mathbf{a}_n + \mathbf{a}_{n+1}) \tag{27}$$

where $\mathbf{d}$, $\mathbf{a}$, $\mathbf{v}$ denote the nodal displacement, acceleration and velocity arrays, respectively.

For the nematic liquid crystal, we can define the internal general force for director field as

$$\mathbf{f}_I^h = -\left\{ \int_{\Omega_0} \mathcal{P}_{i,J} N_{I,J}(\mathbf{X}) \mathbf{e}_i d\Omega + \int_{\Omega_0} \gamma \mathbf{J} \mathbf{r}_i N_I(\mathbf{X}) \mathbf{e}_i d\Omega \right\} \tag{28}$$

where the generalized internal force for the director field is defined as

$$\mathcal{P} = \gamma(\mathbf{F}^{-1} \cdot \mathbf{F}^{-T}) \cdot (\nabla_X \otimes \mathbf{h}) \tag{29}$$

if central difference scheme is used in time integration, we have

$$\mathbf{v}_{n+1}^h = \mathbf{M}_h^{-1} \mathbf{f}_{n+1}^h \tag{30}$$

$$\mathbf{h}_{n+1} = \mathbf{h}_n + \Delta t \mathbf{v}_{n+1}^h. \tag{31}$$

4. Adhesive contact models for cells

Between the cell and its extracellular matrix, there are complex interactions between ligands and receptors. In this research, we do not model the exact molecular mechanism of the adhesion or the detailed molecular motions during this process. Instead, we are interested in modeling the overall adhesion effect between cells and their substrates. The specific attractive adhesion force may be simulated by a cohesive potential, or an attractive potential force, and the

Fig. 3 – A penetrated slave particle and the corresponding master segment.

steric interaction between cell membranes and the substrate is treated as the repulsive force.

We have developed a computational algorithm and modeling techniques to simulate the cell adhesive contacts. The main features of this contact algorithm is (1) using the regular continuum contact mechanics to simulate repulsive force, and (2) using an postulated adhesive potential to mimic attraction force. The continuum contact mechanics algorithm is illustrated in Fig. 3. In the proposed adhesive contact algorithm, the adhesive force is modeled by a special body force that is determined by the distance between a point in the cell and its shortest distance to the substrate as described in Eq. (33). In this case, we do not model the repulsive force, but adopt the conventional finite element or meshfree contact algorithm to enforce the impenetrable condition between the cell and its substrate.

By assuming that the density and the size of the substrate are much larger than the density of the size of the cell, we may neglect the adhesive force from cell to substrate. The total virtual work contribution from the adhesive contact force may be written as

$$\delta\Pi_{AC} = \int_{\Omega_0} B(r)\frac{\mathbf{r}}{r} \cdot \delta\mathbf{u}d\Omega + \int_{\Gamma_c^{(1)}} \mathbf{f}^c \cdot \delta\mathbf{g}dS \tag{32}$$

where the adhesive attraction force is modeled by the following body force

$$B(r) = G\left(\frac{d_0}{r + d_0}\right)^4 \tag{33}$$

where G and d_0 are constants and $\mathbf{r}$ is the distance vector between nodal particles in cell and corresponding surface element in substrate. In adhesive contact, the membrane may be in contact with the ECM. During this process, interpenetration of the cell membrane and the ECM surface is not permitted. The impenetrable condition is enforced to count the repulsive force by using finite element based continuum mechanics contact algorithm. Hence, the second integral in Eq. (33) is a surface integral, in which $\mathbf{g}$ is the gap vector, and $\mathbf{f}^c$ is being modeled as the repulsive normal force + contact frictional force.

The basic idea of classical contact procedure is that the two contacting bodies firstly penetrate into each other within a single explicit time integration step and then additional nodal forces are introduced into the contacting nodal points such that the impenetrability conditions are strictly enforced. We adopted the exact enforcement of the impenetrability condition in a single time step (see Hughes et al., 1976).

In our contact simulations, both cell and ECM can be deformable. Usually the contacting surfaces are designated as

master and slave. We treat the cell outer surface as slaves and treat the ECM top surface as master surface.

The contact algorithm begins with prediction of the slave particles at time step n, the contact–detection algorithm is then used to search all the interpenetration particles based on the determinant value of the meshfree moment matrix (see Li et al., 2001). When penetrations are detected, the next step is to calculate the normal gap and relative tangential velocity between the intrusion slave particles and the closest master surfaces (see Fig. 3). The procedures are outline as followings:

(i): Calculate the normal gap and tangential gap

$$g_j^n = (\mathbf{x}_j^s - \mathbf{x}_i^m) \cdot \mathbf{n}_i \tag{34}$$

$$g_j^t = (\mathbf{x}_j^s - \mathbf{x}_i^m) \cdot \mathbf{t}_i \tag{35}$$

with

$$\mathbf{t}_i = \frac{(\mathbf{x}_{i+1}^m - \mathbf{x}_i^m)}{\|\mathbf{x}_{i+1}^m - \mathbf{x}_i^m\|} \tag{36}$$

$$\mathbf{n}_i = \mathbf{e}_3 \times \mathbf{t}_i \tag{37}$$

where $\mathbf{n}_i$ is the out normal vector of ith master segment matching with the jth penetrated slave particle, $\mathbf{e}_3$ is the unit vector pointing outward from the plane.

(ii): Calculate the normal force and tangential force

The contact force $\mathbf{f}^c$ has two parts: the normal repulsive contact force and the tangential contact friction force.

$$\mathbf{f}_j^n = \frac{2M_j^s g_j}{\Delta t^2} \mathbf{n}_i = f_j^n \mathbf{n}_i. \tag{38}$$

On the tangential direction, the classical Coulomb friction model is adopted in modeling friction between salve body and master body. To enforce the stick condition, we have

$$\mathbf{f}_j^{stick} = -\frac{M_j^s}{\Delta t} \mathbf{v}_j^t. \tag{39}$$

The tangential force cannot exceed the tangential force limit the interface can hold. After reaching the limit, a slip condition should be applied

$$\mathbf{f}_j^{slip} = -|\mu_k f_j^n| \frac{\mathbf{v}_j^t}{\|\mathbf{v}_j^t\|}. \tag{40}$$

The tangential force shall be the minimum of these two forces,

$$\mathbf{f}_j^t = -min(|\mu_k f_j^n|, \|\mathbf{f}_j^{stick}\|) \frac{\mathbf{v}_j^t}{\|\mathbf{v}_j^t\|} \tag{41}$$

where μ_k is the friction coefficient which is decided by different surface materials, $\mathbf{v}_j^t$ is the relative tangential velocity between the jth slave particle and the ith master segment.

(iii): Update the contact force for master contact particles

Since in the simulations the substrate is deformable, we should get the contact force back to the master nodal particles to make sure the total force is balanced. We use a linear interpolation to distribute the contact force to the two nodal particles of the corresponding master segment,

$$\mathbf{f}_i^n = -(1-\alpha)\mathbf{f}_j^n \tag{42}$$

$$\mathbf{f}_i^t = -(1-\alpha)\mathbf{f}_j^t \tag{43}$$

$$\mathbf{f}_{i+1}^n = -\alpha\mathbf{f}_j^n \tag{44}$$

$$\mathbf{f}_{i+1}^t = -\alpha\mathbf{f}_j^t \tag{45}$$

where

$$\alpha = \frac{g_j^t}{\|\mathbf{x}_{i+1}^m - \mathbf{x}_i^m\|}, \quad (0 \leq \alpha < 1) \tag{46}$$

(iv): Redistribute the contact forces to neighboring particles within the support

The force vectors calculated above are the exact nodal force vector for each penetrating slave particle and corresponding master nodal surface particles. In meshfree approach, we have to redistribute such exact nodal force to its supporting nodal particles. Hence after the force distribution, the contact force at the particle I is,

$$\bar{\mathbf{f}}_I = \sum_{J=1}^{n_{node}} N_I(\mathbf{X}_J)\mathbf{f}_J. \tag{47}$$

In finite element interpolation, $N_I(\mathbf{X}_J) = \delta_{IJ}$, we recover the exact nodal force vector.

In actual cell contact, the spatial densities for both ligands and receptors changes from time to time during the adhesive contact. In fact, both ligands and receptors are capable of self-assemble, which is a complex mechano-diffusion process e.g. Freund and Lin (2004).

We hypothesize that the density of the receptors is directly related to the spatial density and magnitude of director field of liquid crystal field, such that the weak forms of Eqs. (16) and (17) are explicitly coupled through the spatial density and magnitude of the directory field, i.e. $\beta_1(t) = c_1 \rho^d(t)\|\mathbf{h}\|$ and $\beta_2(t) = c_2 \rho^d(t)\|\mathbf{h}\|$ where c_1 and c_2 are constants. A coupled mechano-diffusive contact/adhesion theory for the soft matter cell model will be presented in a separated paper. As a preliminary study, in this paper, we consider that the densities of ligands and receptors in the contact zone are fixed.

In this work, the interaction zone between ligands and receptors is modeled as an interactive zone that separates the cell and its substrate, and the adhesive body force distribution varies according to the magnitude of the gap distribution. The adhesive interaction is strong near the contact zone, and it decays after a material point is away from the contact zone. The attractive part of the adhesive contact model is similar to a special version of the coarse-grain FEM adhesion contact algorithm proposed for long range van der Waals force by Sauer and Li (2007). For detailed information of coarse-graining adhesion model, readers may consult Sauer and Li (2007).
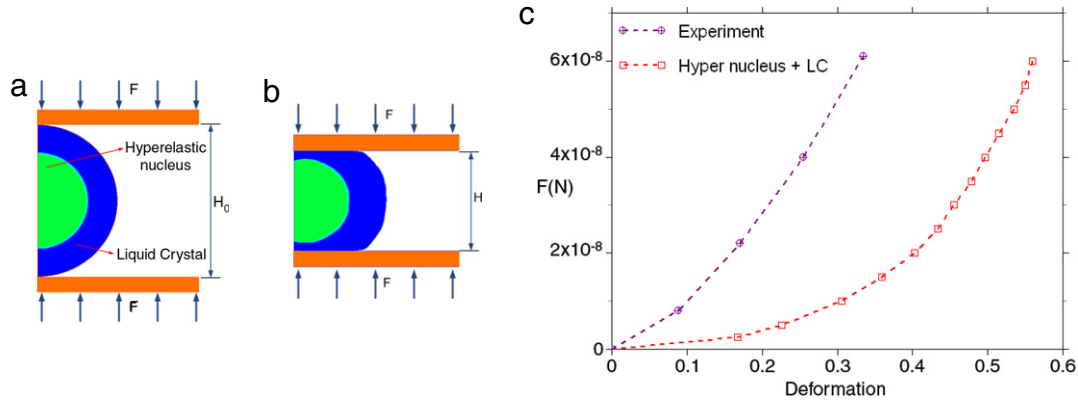
Fig. 4 – Validation of the cell model: (a) Before deformation; (b) After deformation; (c) Force–deformation curve.

5. Numerical simulations

We have applied the soft matter cell model together with the multiscale contact–adhesion algorithm to simulate cell–ECM contact and adhesion. To ensure a meaningful simulation, we have first conducted validation test of the proposed cell model. By doing so, we can identify the parameters of the soft matter model. Then we applied the verified material model to simulate contact between a cell and substrates with different stiffness. We have also simulated the interaction between the cell and a substrate that has non-uniform stiffness.

5.1. Validation of the material models

To validate the proposed cell model, we have applied it to simulate cell deformation under compression and compared with experiment measurements for endothelial cells (Caille et al., 2002). The cell nucleus is modeled as hyperelastic Mooney–Rivlin material and outside of the nucleus region is modeled as nematic liquid crystal. The constant force is applied at the top and bottom rigid microplates, and the boundary nodes are in contact with the cell surface. The classical contact algorithm is applied in the two contact surfaces. In the simulation, the cell deformation is defined as the relative reduction in height, i.e. $(H_0 - H)/H_0$. Fig. 4(a) and (b) show the cell shape before and after deformation. The force–deformation curve is plotted in Fig. 4(c). The applied compressive forces increases nonlinearly as a function of the cell height reduction. From the simulation, one can find that the force required to create the same deformation for endothelial cell is larger than stem cells, which is reasonable considering the stem cells is undeveloped cells.

Since endothelial cells are not stem cells, so it is very hard for us to fit the model with the experimental data obtained from endothelial cells. It can be seen from Fig. 4 that our stem cell model is much softer than endothelial cells, which most likely is true in reality.

5.2. Cell response in four different stiffness substrates

The cell is modeled as a circular plate for 2D, a ball for 3D, with a diameter of $D = 10$ μm. The substrate is modeled as
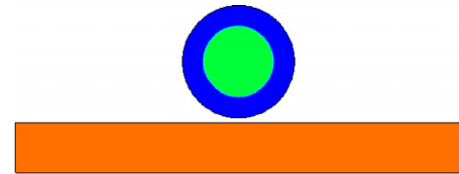

Fig. 5 – Computational model of cell spreading on different substrates (different colors stand for different material models).

a 2D plate with a dimension of ($L \times H = 39.78$ μm $\times 4.5$ μm). The exact problem statement is shown in Fig. 5. Plain strain is assumed in our simulations.

In meshfree computation, a total of 4455 particles are used in discretization of the cell, and 5525 particles are used to form the meshfree discretization of the substrate. The time step is chosen as $\Delta t = 5 \times 10^{-12}$ s. The dilation parameters are selected as ($\rho_x = 1.48\Delta x$, $\rho_y = 1.48\Delta y$) and ($\Delta x = 0.174$ μm, $\Delta y = 0.2$ μm) for cell, ($\Delta x = 0.18$ μm, $\Delta y = 0.18$ μm) for substrate. The nucleus of the cell is modeled as hyperelastic Mooney–Rivlin material. The initial density is $\rho^0 = 1.0 \times 10^3$ kg/m^3 and the material constants are $C_1^n = 2.126 \times 10^3$ Pa, $C_2^n = 1.700 \times 10^2$ Pa and $\lambda^n = 1.700 \times 10^5$ Pa. The region beyond the hyperelastic nucleus is modeled as nematic liquid crystal. The density of the liquid crystal is chosen as $\rho^0 = 1.0 \times 10^3$ kg/m^3, the density of the director field is $\rho_d^0 = 1.0$ and the material properties and constants are $\kappa = 2.2 \times 10^9$ Pa, $\mu = 1.0 \times 10^{-3}$ kg/(m s), $\eta = 5.0 \times 10^{-8}$, $\varepsilon = 1.0 \times 10^{-6}$, $\gamma = 1.0 \times 10^{-4}$. The friction coefficient for the contact algorithm is chosen as $\mu_k = 0.1$. The substrate is modeled as hyperelastic Mooney–Rivlin material. Four different substrates with different stiffness are considered. The density for four substrates are same as the cell nucleus. We set the material constants $C_1 = 1.265 \times 10^4$ Pa, $C_2 = 1.012 \times 10^3$ Pa and $\lambda = 1.012 \times 10^6$ Pa. The material properties for four different substrates are chosen as:

$$C_1^{S1} = C_1, \quad C_1^{S2} = 2C_1, \quad C_1^{S3} = 5C_1, \quad C_1^{S4} = 10C_1$$
$$C_2^{S1} = C_2, \quad C_2^{S2} = 2C_2, \quad C_2^{S3} = 5C_2, \quad C_2^{S4} = 10C_2$$
$$\lambda^{S1} = \lambda, \quad \lambda^{S2} = 2\lambda, \quad \lambda^{S3} = 5\lambda, \quad \lambda^{S4} = 10\lambda.$$

The classical continuum contact algorithm has been used in these simulations. The constant $G = 9.8 \times 10^6$ N/kg and $d_0 =$
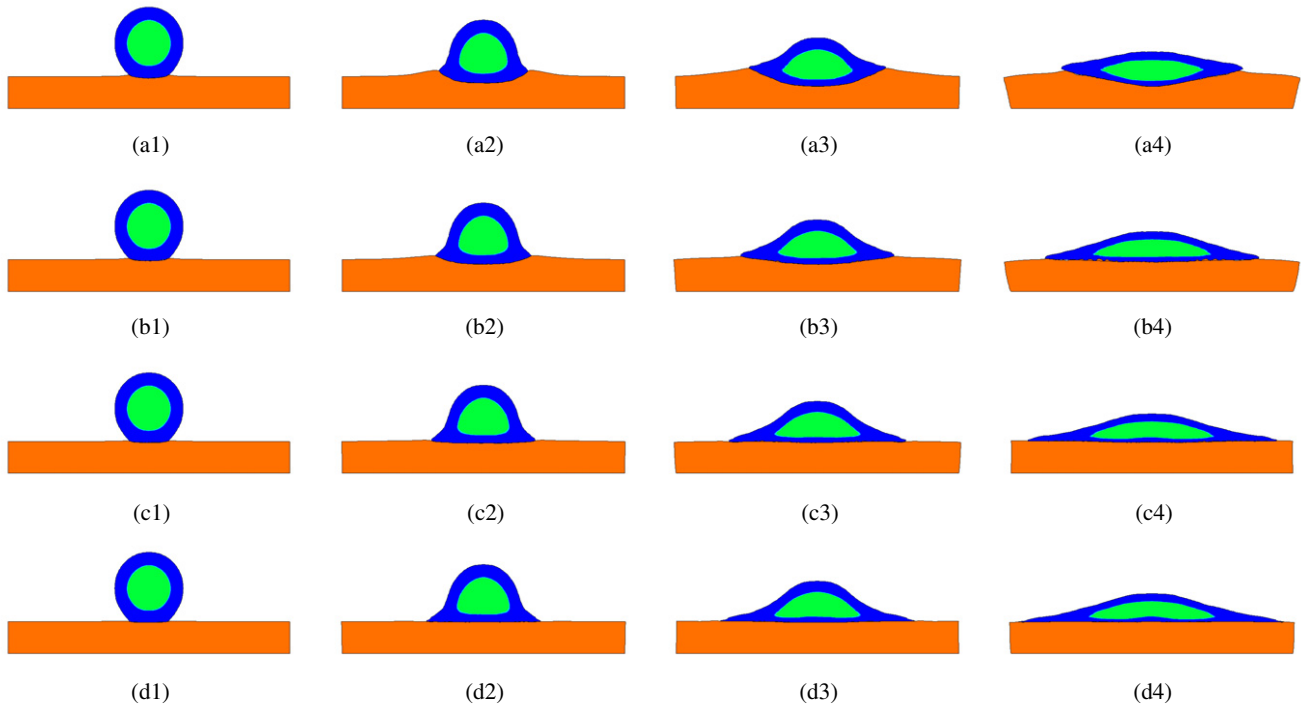
Fig. 6 – Cell spreading over substrates with different stiffness: (a) Substrate-I, (b) Substrate-II, (c) Substrate-III, (d) Substrate-IV.

4.0×10^{-5} m for the adhesive body force (see Eq. (33)). The cell is standing still initially and the initial gap between the cell and substrate is 400 nm. The bottom surface of the substrate is fixed during the whole simulation time. The adhesive force will bring the cell into contact with the substrate, and then the cell will spread under the adhesive and contact forces. Simulations have been carried out for cells in contact with four substrates of different elastic modulus (stiffness) described above.

From this simulation, one may observe the cell spreading over time. In Fig. 6, we display the cell shapes on four different substrates with different stiffness under the same contact conditions at the same time. One may find that the contact between the cell and softest substrate (substrate-I) (Fig. 6 (a)) generates the least cell spreading, and the contact between the cell and substrate-II (Fig. 6(b)) has the second least cell spreading, and the contact between the cell and substrate-III (Fig. 6(c)) has the second most spreading, and when we keep increasing the substrate stiffness, the cell on the substrate-IV has the most spreading (Fig. 6(d)).

It may be noted that although the case IV generates the most cell spreading, the difference between Case IV and Case III is very small, which means the spreading may not increase any more when the stiffness of the substrate reaches a certain value. However, within certain range, cell spreading area is directly related to the stiffness of the substrate, and it is purely a phenomenon of soft elasticity. Based on this model, the stem cell is a mechanical sensor, and it can translate the mechanical information (properties) of the substrate into its shape, configuration, and size. This is the definition of mechanotransduction.

Zooming in Fig. 6, we juxtapose the two last sequences of cell contact process in Fig. 7. From Fig. 7 (b), one may

find that under stiff substrate the shape of the cell nucleus become concave in contract of the convex shape of the cell nucleus under softer substrates. This finding indicates that the deformed shape of cell nucleus also depend on the stiffness of the extracellular matrix. This is a first concrete evidence of cell mechanotransduction at a distance without using the explanation of the tensegrity postulate on the structure of cell scaffold (see Wang et al., 2009). In fact, embryonic stem cells do not have well-developed cell scaffold structures. To the best of authors' knowledge, this type of cell response has not been reported before.

5.3. Cell response in a stiffness-varying substrate

It is interesting to consider cell contact with substrate that has non-uniform stiffness. We set the material properties in the substrate as a function of position x to observe the cell spreading motion in different directions

$$C_1^S = C_1(0.1 + 9.9r)$$
$$C_2^S = C_2(0.1 + 9.9r)$$
$$\lambda^S = \lambda(0.1 + 9.9r)$$

where r is defined as: $r = (x + L/2)/L$ with the center of the substrate at $x = 0$. The exact problem statement is shown in Fig. 8. In Fig. 9, we display a time sequence of a cell contacting with a stiffness-varying deformable substrate. The color contour is the effective stress contour. Without varying the stiffness, the cell should move equally on both left and right side of the substrate. From the simulation results, one can find immediately that cell move towards the right side much faster than to the left side of the substrate due

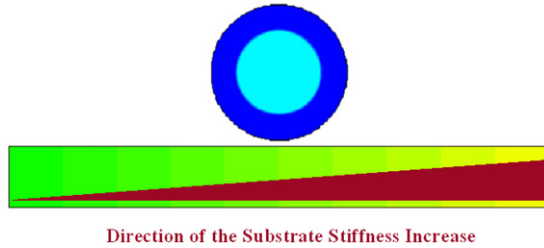**Fig. 7 – Cell nucleus configurations with different ECM stiffness:** (a) = b4; (b) = d4.

Fig. 8 – Computational model of cell spreading on a stiffness-varying substrate.

to the stiffness gradient, which means that the cell is in favor of stiffer substrate. This results agreed very well with experimental measurement (Wong et al., 2003), (Engler et al., 2006) and numerical simulations (Ni and Chiang, 2007) of cell adhesion and migration.

6.   Discussions and conclusions

In conclusion, the proposed soft matter cell model may be applicable to simulation of stem cell contact providing possible explanations on cell mechanotransduction and other issues at the large scale level.

Our simulations have shown that: (1) By using the proposed soft matter cell model, when a "cell" is in contact with a substrate, its traction force may change depending on stiffness of the substrate; (2) the size of spreading area of the cell also changes or differs depending on the stiffness of extracellular substrate (see Fig. 6); and (3) during soft contact process, the cell is in favor of stiffer substrate (see Fig. 9). It should be noted that cell, in particular stem cell, behaviors are complex biological phenomena. The proposed soft matter cell model is only intended to model mechanical behaviors of cells at a coarse-gaining level, which may not and cannot explain the molecular mechanisms of cell motion, evolution, and proliferation, and it requires in depth study of every aspects of molecular cell biology including all relevant bio-chemical, bio-physical, as well as bio-mechanical factors and their interactions at different scales.

Developing soft matter models for cells especially stem cells may help us understand bio-mechanical and bio-physical behaviors of cells. It has been shown in this paper that the soft matter model can offer much more explanations on interaction between the stem cell and its mechanical niche than that of the hyperelastic cell model. In some cases, the soft matter model has even shown its predictive power. It is the authors' opinion that by combining the soft matter cell model with molecular simulation we may be able to achieved qualitative prediction on cell behaviors in collaborating with experimental observation. The predictive stem cell model may provide both scientific insight as well as clinic guidance on a host of health care problems, such as regenerated medicine and drug design and delivery problems.
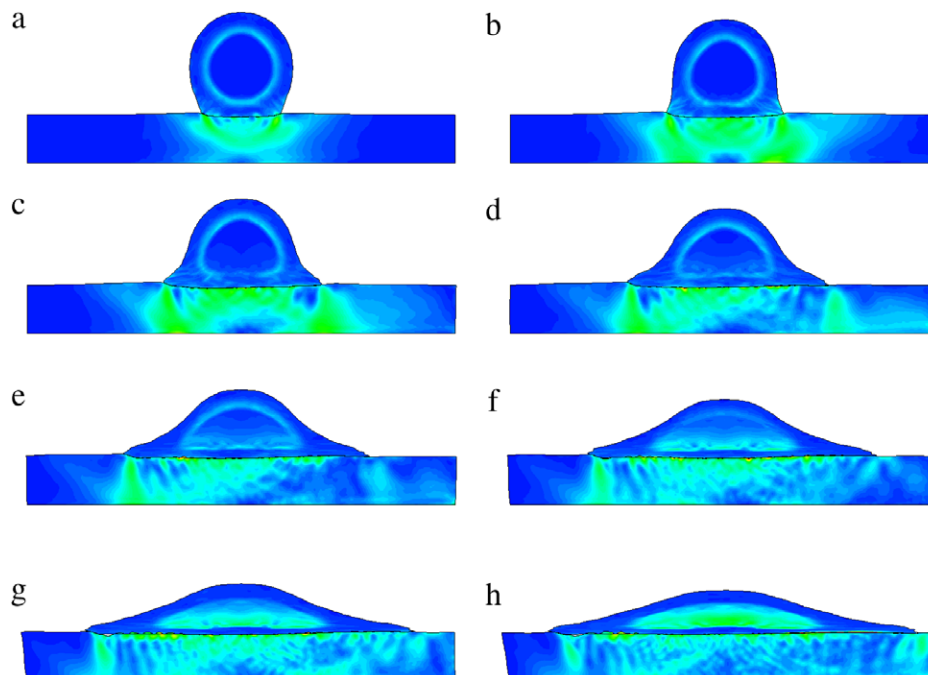

Fig. 9 – Time sequence of cell contact with a stiffness-varying substrate.

The soft matter cell model presented in this work is a primitive one, but it may have provided a useful approach for more realistic and more accurate modeling of cells, especially stem cells. It is possible that along the line more sophisticated soft matter models can be made that are capable of simulating self-assembly of focal adhesion, cell division, proliferation and more.

Acknowledgements

REFERENCES

Bao, G., Suresh, S., 2003. Cell and molecular mechanics of biological materials. Nature Materials 2, 715–725.

Caille, N., Thoumine, O., Tardy, Y., Meister, J., 2002. Contribution of the nucleus to the mechanical properties of endothelial cells. Journal of Biomechanics 35, 177–187.

Cheng, Q.H., Liu, P., Gao, H.J., Zhang, Y.W., 2009. A computational modeling for micropipette-manipulated cell detachment from a substrate mediated by receptorCligand binding. Journal of the Mechanics and Physics of Solids 57 (2), 205–220.

Chien, S., 2007. Mechanotransduction and endothelial cell homeostasis: the wisdom of the cell. American Journal of Physiology Heart Circulation Physiology 292, H1209–H1224.

Damjanovich, S., Gaspar Jr., R., Pieri, C., 1997. Dynamic receptor superstructures at the plasma membrane. Quarterly Reviews of Biophysics 30, 67–106.

Deshpande, V.S., Mrksich, M., McMeeking, R.M., Evans, A.G., 2008. A bio-mechanical model for coupling cell contractility with focal adhesion formation. Journal of the Mechanics and Physics of Solids 56, 1484–1510.

Dietrich, C., Yang, B., Fujiwara, T., Kusumi, A., Jacobson, K., 2002. Relationship of lipid rafts to transient confinement zones detected by single particle tracking. Biophysical Journal 82, 274–284.

Discher, D.E., Janmey, P., Wang, Y.L., 2005. Tissue cells feel and respond to the stiffness of their substrate. Science 310, 1139–1143.

Discher, D.E., Mooney, D.J., Zandstra, P.W., 2009. Growth factirs, matrices, and forces combine and control stem cells. Science 324, 1673–1677.

Engler, A.J., Sen, S., Sweeney, H.L., Discher, D.E., 2006. Matrix elasticity directs stem cell lineage specification. Cell 126, 677–689.

Fereol, S., Fodil, R., Laurent, V.M., Balland, M., Louis, B., Pelle, G., Hnon, S., Planus, E., Isabey, D., 2009. Prestress and adhesion site dynamics control cell sensitivity to extracellular stiffness. Biophysical Journal 96, 2009–2022.

Freund, L.B., Lin, Y., 2004. The role of binder mobility in spontaneous adhesive contact and implications for cell adhesion. Journal of the Mechanics and Physics of Solids 52, 2455–2472.

Fried, I., Johnson, A.R., 1988. A note on elastic energy density functions for largely deformed compressible rubber solids. Computer Methods in Applied Mechanics and Engineering 69, 53–64.

Helfrich, W., 1973. Elastic properties of lipid bilayer: theory and possible experiments. Zeitschrift fuer Naturforschung B (Chemical Sciences) 28, 693–703.

Hughes, T.J.R., Talor, R., Sackman, J., Curnier, A., Kanoknukulchai, W., 1976. A finite element method for a class of contact-impact problem. Computer Methods in Applied Mechanics and Engineering 8, 249–276.

Jacobson, K., Sheets, E.D., Simson, R., 1995. Revisiting the fluid mosaic model of membranes. Science 268, 1441–1442.

Li, S., Qian, D., Liu, W.K., Belytschko, T., 2001. A meshfree contact-detection algorithm. Computer Methods in Applied Mechanics and Engineering 190, 3271–3292.

Li, S., Liu, W.K., 2004. Meshfree Particle Methods. Springer, Berlin.

Lin, F.H., Liu, C., 2000. Existence of solutions for the Ericksen-Leslie system. Archive for Rational Mechanics and Analysis 154, 135–156.

Liu, P., Zhang, Y.W., Cheng, Q.H., Lu, C., 2007. Simulations of the spreading of a vesicle on a substrate surface mediated by receptor-ligand binding. Journal of the Mechanics and Physics of Solids 55, 1166–1181.

Maniotis, A.J., Chen, C.S., Ingber, D.E., 1997. Demonstration of mechanical connections between integrins, cytoskeletal filaments, and nucleoplasm that stabilize nuclear structure. Proceeding of the National Academy of Sciences of the United States of America 94, 849–854.

Ni, Y., Chiang, Martin Y.M., 2007. Cell morphology and migration linked to substrate rigidity. Soft matter 3, 1285–1292.

Rehfelt, F., Engler, A.J., Eckhardt, A., Ahmed, F., Discher, D.E., 2007. Cell responses to the mechanochemical micro-environment — Implications for regenerative medicine and drug delivery. Advancesd Drug Delivery Reviews 59, 1329–1339.

Sauer, R., Li, S., 2007. A contact mechanics model for quasi-continua. International Journal for Numerical Methods in Engineering 71, 931–962.

Sen, S., Engler, A.J., Discher, D.E., 2009. Matrix strains induced by cells: computing how far cells can feel. Cellular and Molecular Bioengineering 2, 39–48.

Singer, S.J., Nicolson, G.L., 1972. The fluid mosaic model of the structure of cell membranes. Science 175, 720–731.

Sun, L., Cheng, Q.H., Gao, H.J., Zhang, Y.W., 2009. Computational modeling for cell spreading on a substrate mediated by specific interactions, long-range recruiting interactions, and diffusion of binders. Physical Review E 79, 061907.

Vereb, G., Szolosi, J., Matko, J., Nagy, P., Farkas, T., Vigh, L., Matyus, L., Waldmann, T.A., Damjanovich, S., 2003. Dynamic, yet structured: The cell membrane three decades after the Singer-Nicolson model. Proceedings of the National Academy of Sciences of the United States of America 100 (14), 8053–8058.

Wang, N., Tytell, J.D., Ingber, D.E., 2009. Mechanotransduction at a distance: mechanically coupling the extracellular matrix with the nucleus. Nature Reviews Molecular Cell Biology 10, 75–82.

Wong, J.Y., Velasco, A., Rajagopalan, P., Pham, Q., 2003. Directed movement of vascular smooth muscle cells on gradient-compliant hydrogels. Langmuir 19, 1908–1913.

Wozniak, M.A., Chen, C.S., 2009. Mechanotransduction in development: a growing role for contractility. Nature Reviews – Molecular Cell Biology 43, 34–43.